

Article

**Phenolic bis-styrylbenzo[c]-1,2,5-thiadiazoles as probes for
fluorescence microscope mapping of A β plaque heterogeneity**

Jun Zhang, Audun Konsmo, Alexander Sandberg, Xiongyu Wu, Sofie Nyström, Ulrike Obermueller,
Bettina M Wegenast-Braun, Peter Konradsson, Mikael Lindgren, and Per Hammarström

J. Med. Chem., **Just Accepted Manuscript** • DOI: 10.1021/acs.jmedchem.8b01681 • Publication Date (Web): 01 Feb 2019

Downloaded from <http://pubs.acs.org> on February 2, 2019

Just Accepted

"Just Accepted" manuscripts have been peer-reviewed and accepted for publication. They are posted online prior to technical editing, formatting for publication and author proofing. The American Chemical Society provides "Just Accepted" as a service to the research community to expedite the dissemination of scientific material as soon as possible after acceptance. "Just Accepted" manuscripts appear in full in PDF format accompanied by an HTML abstract. "Just Accepted" manuscripts have been fully peer reviewed, but should not be considered the official version of record. They are citable by the Digital Object Identifier (DOI®). "Just Accepted" is an optional service offered to authors. Therefore, the "Just Accepted" Web site may not include all articles that will be published in the journal. After a manuscript is technically edited and formatted, it will be removed from the "Just Accepted" Web site and published as an ASAP article. Note that technical editing may introduce minor changes to the manuscript text and/or graphics which could affect content, and all legal disclaimers and ethical guidelines that apply to the journal pertain. ACS cannot be held responsible for errors or consequences arising from the use of information contained in these "Just Accepted" manuscripts.



ACS Publications

is published by the American Chemical Society, 1155 Sixteenth Street N.W.,
Washington, DC 20036

Published by American Chemical Society. Copyright © American Chemical Society.
However, no copyright claim is made to original U.S. Government works, or works
produced by employees of any Commonwealth realm Crown government in the course
of their duties.

Phenolic bis-styrylbenzo[c]-1,2,5-thiadiazoles as probes for fluorescence microscope mapping of Aβ plaque heterogeneity

Jun Zhang,^[a] Audun Konsmo,^[b] Alexander Sandberg,^[a] Xiongyu Wu,^[a] Sofie Nyström,^[a] Ulrike Obermüller,^[c,d] Bettina M. Wegenast-Braun,^[c,d] Peter Konradsson,^[a] Mikael Lindgren,^[b] and Per Hammarström,^{*[a]}

^[a]Division of Chemistry, Department of Physics Chemistry and Biology, Linköping University, 581 83 Linköping, Sweden

^[b]Department of Physics, Norwegian University of Science and Technology, 7491 Trondheim, Norway

^[c]Department of Cellular Neurology, Hertie Institute for Clinical Brain Research, University of Tübingen, 72076 Tübingen, Germany

^[d]DZNE–German Center for Neurodegenerative Diseases, 72076 Tübingen, Germany

*Corresponding author: per.hammarstrom@liu.se

ABSTRACT

A fluorescent bis-styryl-benzothiadiazole (BTD) with carboxylic acid functional groups (X-34/Congo red analogue) had lower binding affinity towards A β 1-42 and A β 1-40 fibrils than its neutral analogue. Hence, variable patterns of neutral OH substituted bis-styryl-BTDs were generated. All bis-styryl-BTDs showed higher binding affinity to A β 1-42 fibrils than to A β 1-40 fibrils. The *para*-OH on the phenyl rings was beneficial for binding affinity while a *meta*-OH decreased the affinity. Differential staining of transgenic mouse A β amyloid plaque cores compared to peripheral coronas using neutral compared to anionic bis-styryl ligands indicate differential recognition of amyloid polymorphs. Hyperspectral imaging of transgenic mouse A β plaque stained with uncharged *para*-hydroxyl substituted bis-styryl-BTD implicated differences in binding site polarity of polymorphic amyloid plaque. Most properties of the corresponding bis-styryl-BTD was retained with a rigid alkyne linker rendering a probe insensitive to cis-trans isomerization. These new BTD-based ligands are promising probes for spectral imaging of different A β fibril polymorphs.

INTRODUCTION

Alzheimer's disease (AD) is a common neurodegenerative disorder and a leading cause of dementia among older adults.¹⁻² Extracellular senile plaques and intracellular neuro-fibrillary tangles (NFTs), the main two pathological hall-marks of AD, are composed of fibrous amyloid- β peptides (mainly A β 1-40 and A β 1-42) and abnormally hyperphosphorylated tau protein, respectively.³⁻⁵ To date, various small molecular scaffolds targeting the regular cross β -pleated sheet conformation of protein aggregates have been developed.⁶⁻⁹ In this regard, the pan-amyloid targeting molecule X-34 [2,5-bis(4'-hydroxy-3'-carboxy-styryl)benzene, see Chart 1], is an important scaffold for amyloid fibril probe development.¹⁰ Congo red, the gold standard for amyloid diagnostics, was used as starting scaffold for the design of X-34 by the Klunk group. Congo red carries anionic sulfonic acid moieties as terminal groups and have been shown to direct specific interactions with amyloid fibril binding sites.¹¹ In contrast, uncharged analogues K114, DF-9 and Methoxy-X04, which have been shown to penetrate the blood-brain barrier (BBB) still bind to A β plaques deposited in APP or APP/PS1 mice,¹²⁻¹⁶ as well as to amyloid fibrils in human tissues.¹² These results show that anionic functional groups are not necessary for good A β -fibril binding. As research tools fluorescent amyloid dyes are indispensable. In particular Methoxy-X04 has been extensively utilized for quantitative 2-photon fluorescence *in vivo* imaging of amyloid plaque formation in APP transgenic mice.¹⁷⁻¹⁸

π -extended 2,1,3-benzothiadiazole (BTD) derivatives are a new class of bio-probes with attractive photophysical properties: high molar extinction coefficients, large Stokes shifts, high quantum yields, high storage stability, bright emission, good signal-to-noise ratios, efficiency to cross the cell membranes and low fading after long periods of irradiation.¹⁹ Although a large number of fluorescent small molecule BTD derivatives were applied to bioimaging analyses of

several cell types, little is known about this class of bio-probes used to stain A β plaques and NFTs. Nilsson and coworkers reported on L3 (Chart 1), which can intensely stain A β plaques,²⁰ and HS-169 (Figure 1), intensely stain A β plaques and NFTs.²¹ In addition, we recently reported that BTDSB, a derivative of salicylate bis-styrylbenzene X-34 (Chart 1) displayed emission in the red region (620 nm) with a long Stokes shift (133 nm). It was also shown to have high binding affinity (K_d : 93 ± 5 nM) when bound to recombinant A β 1-42 fibrils and intensely stained both A β plaques and NFTs in AD brain tissue sections.²²

As a starting point for our studies we compared the differential staining of individual plaque using uncharged DF-9, in comparison with the analogous anionic X-34, known to target the Congo red binding site. Interestingly, variations in plaque staining implicated differential targeting of amyloid structures of these ligands. We then redesigned bis-styryl-BTD ligands with modification of the outer phenyl ring using various hydroxyl motifs investigating A β fibril binding affinity (A β 1-42 and A β 1-40) and specificity. The *para*-substituted bis-styryl-BTD showed superior affinity and was particularly sensitive to binding site polarity, suggesting additional amyloid polymorph sensitivity. A further redesign using an alkyne linker retained high affinity and polarity sensing capacity while removing a potential drawback, i.e. sensitivity towards isomerization of the probe.

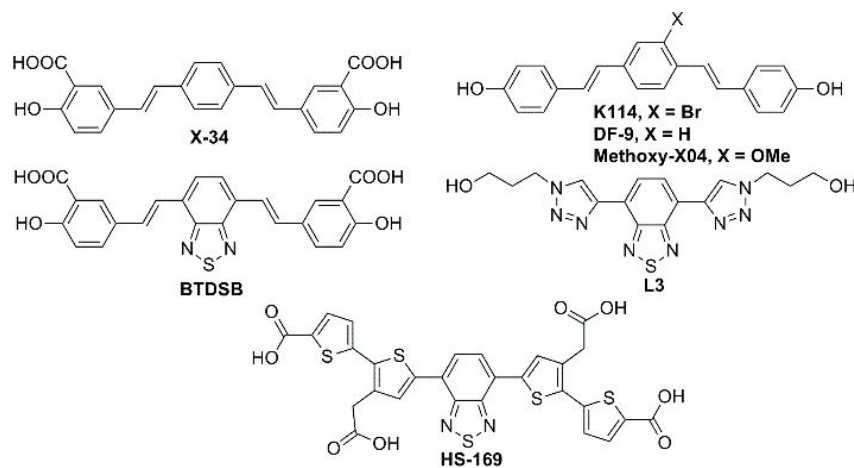


Chart 1. Chemical structures of amyloid ligands reported previously.

RESULTS AND DISCUSSION

Comparison of bis-styryl-benzene carboxylate charge moieties for fibril targeting. Anionic charges have been shown to be important for specific targeting the Congo red binding site of amyloid fibrils. We took advantage of the different excitation and emission spectra of our previously reported BTDSB probe and X-34 and DF-9 to compare amyloid binding sites. X-34 and BTDSB bind to the same binding site²² and as expected, we observe mainly co-localized staining of these probes on sections of APP23 mice with amyloid plaque (Figure 1A). In contrast, co-staining with DF-9 and BTDSB showed vastly different staining patterns with DF-9 bound to the core of the plaque while BTDSB dominated the periphery (Figure 1B). This is interesting, because it is known that aged APP23 mice (>18 months) show polymorphic amyloid structures within individual neuritic plaque.²³⁻²⁴ Co-staining experiments on 5 μ M recombinant A β 1-40 fibrils showed that in the presence of equimolar concentrations (0.5 μ M each) of X-34 and BTDSB, the latter still retained full binding (Figure 1C). DF-9 on the other hand prevented almost 50% of BTDSB binding (Figure 1C). Hence together with the imaging data this proposes that two different binding sites/polymorphs occur on fibrils with varying affinity to uncharged DF-9 in comparison to the known Congo red-type charge mediated binding site targeted by BTDSB and X-34. The DF-9 high affinity polymorph appears mainly in the plaque core because it out competes the negatively charged Congo red analogue BTDSB in the core, but not in the peripheral corona. This suggests that the DF-9 positive core would be the site preferably probed by the analogous neutral trans-stilbene BTD-based ligands of the present study.

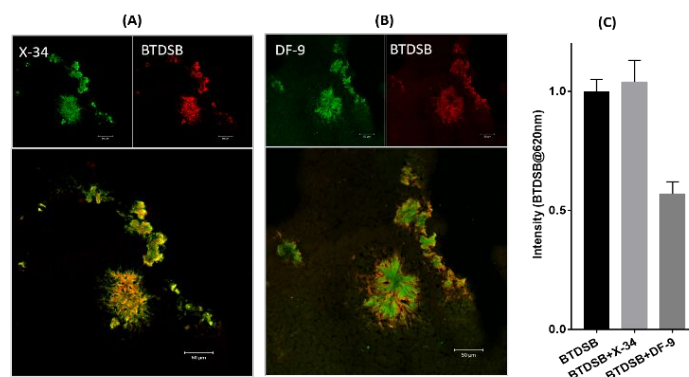
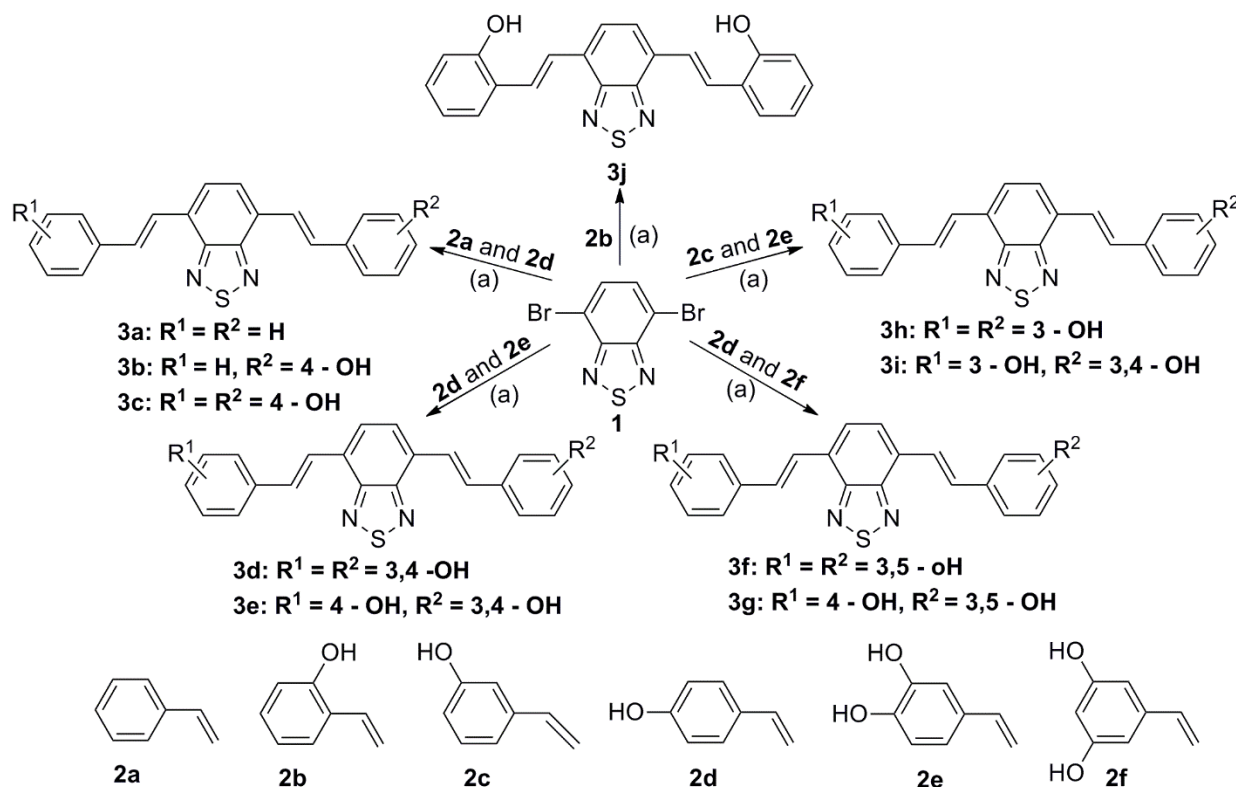


Figure 1. (A) Single plane confocal images of APP23 mouse brain sections (female, 19.5 months) after co-staining with X-34 and BTDSB (top) and the merged image of X-34 and BTDSB (down). (B) after co-staining with DF-9 and BTDSB (top) and the merged image of DF-9 and BTDSB (down). Z-depth was selected for the center of the largest plaque. (C) Competition assays using BTDSB (500 nM) to displace X-34 (or DF-9) in the presence of A β 1-40 fibrils (5 μ M) *in vitro* in PBS (pH 7.4).

Synthesis of bis-styryl-benzothiadiazole ligands and *in vitro* ligand binding with A β 1-42/A β 1-40 fibrils. Compounds **3a** to **3j** were synthesized via the classic Heck reaction using a new one-pot procedure as depicted in Scheme 1. Compounds **2b** to **2f** were prepared via Wittig reaction of the corresponding aldehyde and triphenylphosphine methyl bromide utilizing a previous procedure.²⁵ Compound **2a** was purchased from Sigma-Aldrich. Compound BTDSB was reported previously by our group.²²

Scheme 1. Synthesis of bis-styryl-benzothiadiazole ligands.

Conditions and reagents: (a) $Pd(OAc)_2$, triethanolamine, DMF.

We first investigated the photophysical properties of DF-9 and the BTDA analogue compound **3c** in solution as shown in Figure 2A. Compared with DF-9, **3c** displayed two absorption bands: a high energy band (blue-shift 35 nm) around 340 nm and a low energy band around 485 nm, likely arising from the $\pi-\pi^*$ transition and charge-transfer transition, respectively, similar with that of BTDSB in PBS buffer.²² DF-9 exhibited an emission spectrum with partially resolved vibronic substructure and the maximum at around 440 nm, whereas **3c** showed a broad featureless emission with the peak at 660 nm. **3c** has larger stokes shift (175 nm) than DF-9 (65 nm). We then generated emission spectra of **3a-3j** and BTDSB, DF-9 as a reference, in the presence or absence of monomers and fibrils of A β 1-42 and A β 1-40 (Figure 2B and Figure S1 in supporting information).

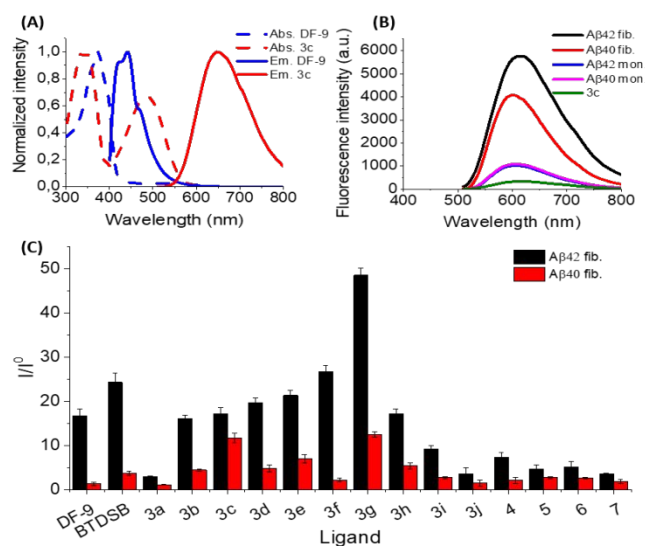
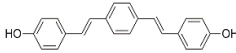
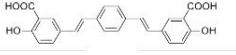
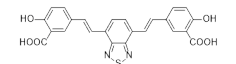
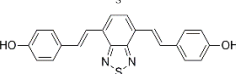
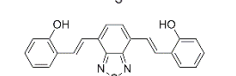
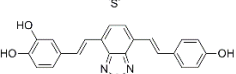
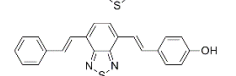
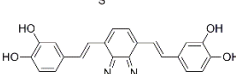
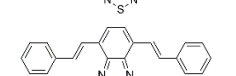
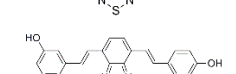
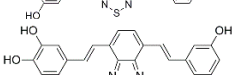
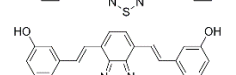
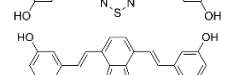


Figure 2. (A) Normalized absorption (dashed) and emission (solid) spectra of DF-9 (blue) and **3c** (red) with 2 μ M in DMSO. (B) Emission spectra of **3c** in the absence or presence of A β 1-42 and A β 1-40 peptides (monomers and fibrils) in PBS buffer. (C) Fluorescence intensity enhancements of **3a** to **3j** and BTDSB as well as DF-9 as control when bound to A β 1-42 or A β 1-40 fibrils compared to free in solution. Excitation wavelengths: 360 nm for DF-9, 430 nm for **4**, 460 nm for **3a**, **3h**, **3f**, **5**, **6**, and 490 nm for all other ligands.

Overall, we found that these ligands showed larger fluorescence intensities when bound to A β 1-42 fibrils than when bound to A β 1-40 fibrils (Figure 2C and Table S1). For several probes weak fluorescence changes were also observed in the presence of A β 1-42 and A β 1-40 monomers in comparison to free ligand (Figure 2B and Figure S1). More details of the binding properties and photophysical characterization are summarized in Table S1.

Next, saturation binding assays were performed to quantitatively evaluate the binding affinity of **3a** to **3j** and BTDSB towards A β 1-42 fibrils and A β 1-40 fibrils, using DF-9 and X-34 as references

Table 1. Binding affinity (K_d) and A β plaque binding specificity (S/N ratio) to A β transgenic mouse brain slices.

compd.	K _d (nM) ^a		S/N ratio ^b		λ _{em} (nm) ^c core/corona	cLogP ^d	τ _{avg} (ns) ^e	
	Aβ1-42	Aβ1-40	plaque core	plaque corona				
DF-9		137±10	58±7	13.7 ± 4.3	31.7 ± 7.6	443/443	6.2	0.7
X-34		149±8 (299±21) ^g	50±4	n.d.	n.d.	n.d.	8.2	0.8 ^f
BTDSB		83 ± 6 (93 ± 5) ^g	250	23.3 ± 2.6	37.4 ± 0.3	614/614	8.1	5.6
3c		20 ± 2	46 ± 2	27.5 ± 1.7	17.3 ± 0.9	574/600	6.0	5.4
3j		29 ± 5	106 ± 22	20.2 ± 0.6	4.5 ± 0.3	565/577	6.0	5.7
3e		31 ± 4	110 ± 22	5.2 ± 0.5	5.3 ± 0.3	573/594	5.4	5.8
3b		39 ± 1	61 ± 17	5.1 ± 0.9	9.3 ± 0.3	575/588	6.7	6.2
3d		39 ± 4	187 ± 8	9.3 ± 2.1	5.2 ± 1.4	571/590	4.8	5.5
3a		66 ± 8	109 ± 19	5.1 ± 0.7	11.5 ± 0.7	548/564	7.3	5.7
3g		73 ± 7	170 ± 13	11.3 ± 1.3	3.3 ± 0.8	594/594	5.3	6.5
3i		77 ± 1	83 ± 20	12.6 ± 1.3	7.7 ± 0.7	575/575	5.4	5.8
3f		95 ± 1	284 ± 12	42.6 ± 5.4	13.4 ± 2.9	566/566	4.7	6.2
3h		116± 10	133 ± 10	2.7 ± 0.5	11.1 ± 0.7	556/563	6.0	5.7

^aValues represent the the average \pm SD of 2 determinations. ^bValues represent the average \pm SD of 10 determinations. ^cEmission maximum of ligand bound to A β plaques (cores and coronas). Images were captured at the center of z-depth focal plane of neuritic plaque cores. ^dCalculated cLogP values using ChemDraw Ultra 12.0 of the fully protonated molecules. ^eMeasured for solute molecule in toluene. ^fMeasured for solute molecule in MeOH. ^gfrom reference.²² n.d. = not determined.

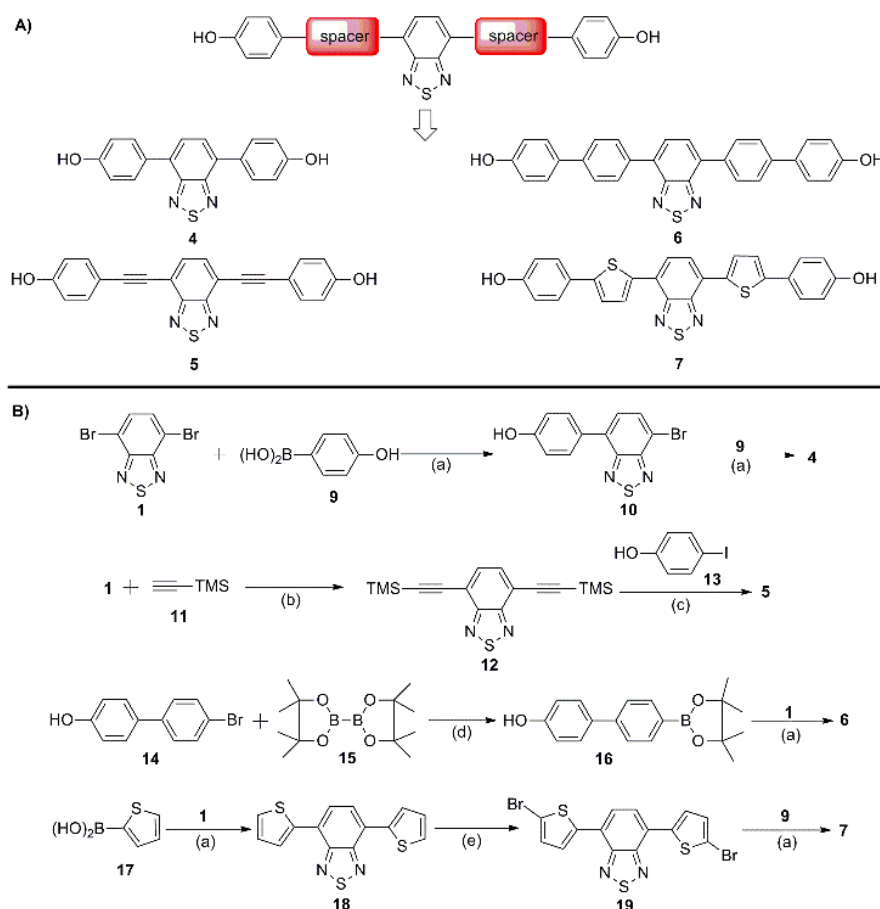
(Table 1 and Figure S2). It is noteworthy that these ligands showed higher binding affinity towards A β 1-42 fibrils compared to A β 1-40 fibrils, which is consistent with their higher fluorescence enhancement with A β 1-42 fibrils. Therefore, we sorted the new BTB compounds in Table 1 following the increase in K_d values towards the A β 1-42 fibrils, and thus, with decreasing binding affinity.

We note that **3c** had the strongest binding affinity (20 ± 2 nM) of all ligands. The binding affinity for **3a** and **3b** was 3.4-fold and 2-fold less compared to **3c**, most likely due to the loss of H-bond stabilization. The K_d data for **3c** versus **3j** and **3h** suggest that the *para*- and *ortho*- are marginally superior to *meta*-substitution on the outer phenyl rings. As evidenced by the 3.4-fold increase in affinity between **3c** and **3a**, 2.3-fold loss of affinity for **3a** compared to **3j**, the *para*-OH on the outer phenyl ring is beneficial to binding affinity while the *meta*-OH decreases the binding affinity, supported by the K_d data for **3h** versus **3i** versus **3d**. Although the *meta*-OH could decrease the binding affinity, **3f** showed higher binding affinity compared to **3h**, attributed to the 2 more of H-bond stabilization by the phenol functional group. As evidenced by the 4.3-fold loss in binding affinity for BTDSB compared to **3c**, the carboxylic acid functional groups decreased the affinity, suggesting that acidic functional groups are not required for good A β binding, which is in line with X-34 (299 ± 21 nM)²² versus DF-9 (137 ± 10 nM) for A β 1-42 fibrils and comparable affinities for A β 1-40 fibrils.

Synthesis and photophysical properties of benzothiadiazole based amyloid ligands with various conjugated spacers. A known issue with *trans*-stilbenes is the *cis-trans* isomerization of the vinyl bond. We hence explored *para*-substituted mono-hydroxyl BTB variants with variable conjugated spacers. The synthesis of **4** to **7** was performed by means of palladium-catalyzed coupling reactions of 4,7-dibromo-2,1,3-benzothiadiazole (**1**) (Scheme 2) Compounds **12**, **16**, **18**

and **19** were obtained using previously reported procedures.²⁵⁻²⁷ Compounds **4**, **6** and **7**, which possessed distinct spacers such as thiophene and benzene, were obtained vis Suzuki reaction of **1** with arylboronic acid or arylboronic ester. The Sonogashira coupling reaction of **1** with trimethylsilylacetylene (**11**) gave 4,7-diethynyl-2,1,3-benzothiadiazole (**12**), which was derived to **5** by reaction with 4-iodophenol (**13**).

Scheme 2. Synthesis of BTD derivatives with different conjugated spacers^a



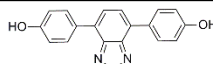
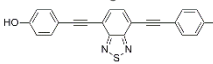
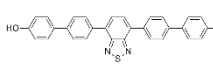
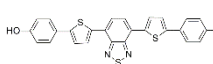
^a Conditions and reagents: (a) Pd(PPh₃)₄, 2 M Na₂CO₃, benzene-EtOH, 90 °C; (b) Pd(PPh₃)₄, CuI, triethylamine, 75 °C; (c) 1) KOH in MeOH rt; 2) Pd(OAc)₂, PPh₃, CuI, triethylamine, THF, rt; (d) PdCl₂(dppf), dppf, KOAc, 1,4-dioxane, 90 °C; (e) NBS, CHCl₃, rt.

The photophysical properties of compounds **4** to **7** and **3c** were measured in PBS buffer (pH 7.4). The normalized absorption and emission spectra are shown in Figure S3 and the results in terms of spectroscopic parameters are summarized in Table S2. As expected, all ligands showed two absorption bands: a high energy band and a low energy band, likely arising from the π - π^* transition and charge-transfer transition, respectively. Compounds **4**, **5** and **6** displayed very similar absorption spectra with the maximum wavelength at 402 nm, 404 nm and 400 nm, respectively, indicating that C-C single bond, C \equiv C triple bond and a benzene ring as conjugated spacers gives a similar electronic transition from S0 to S1 localized to the BTD group. Compounds **3c** and **7** have their absorption maxima at 432 and 486 nm, respectively, demonstrating that the transition is delocalized to the thiophene ring more efficiently than e.g., the C=C double bond. All ligands showed very weak emission in PBS buffer with emission maxima ranging from 545 nm for **6** up to 660 nm for **7** because of the strong intermolecular interactions of electric dipole and π - π stacking propensity.²⁸ It is worth noting that all BTD based ligands show longer emission wavelengths (545-670 nm) than that of DF-9 (440 nm) and have large stokes shift in solution, 146-202 nm, allowing unambiguous detection without reabsorption effects and not interfering with the background fluorescence of biomolecules at the blue end of the spectrum (FAD and NADH peaks at approx. 450-520nm).²⁹

***In vitro* ligand binding assays of **4** – **7** with A β 1-42/A β 1-40 fibrils:** We investigated the emission behavior of **4** to **7** with monomers and fibrillar aggregates of A β 1-42 and A β 1-40 peptides (Figure S4). These probes showed an apparent fluorescence intensity with significant hypsochromic shift (Figure 2C and Table S3) in the presence of A β 1-42 fibrils than that when bound to A β 1-40 fibrils, demonstrating that these probes are more sensitive to A β 1-42 fibrils over than A β 1-40 fibrils. However, relative weak fluorescence changes were observed in the presence

of freshly monomerized Aβ1-42 and Aβ1-40 peptides. It should be noted that upon binding to Aβ1-42 fibrils, these probes displayed long emission wavelengths, especially **7** (655 nm).

Table 2. Binding affinity (K_d) and Aβ plaque binding specificity (S/N ratio) to Aβ transgenic mouse brain slices

compd.	K_d (nM) ^a		S/N ratio ^b		λ_{em} (nm) ^c core/corona	cLogP ^d	τ_{avg} (ns) ^e
	Aβ1-42	Aβ1-40	plaque core	plaque corona			
4 	511 ± 29	250 ± 25	17.4 ± 1.2	5.9 ± 0.4	545/557	4.4	8.4
5 	36 ± 3	59 ± 5	17.4 ± 2.4	23.2 ± 1.3	537/562	5.9	3.4
6 	40 ± 4	> 400	~ 1	~ 1		8.2	4.4
7 	10 ± 1	> 400	5.4 ± 0.6	2.9 ± 0.2	630/630	8.4	5.4

^a Values represent the average ± SD of 2 determinations. ^b Values represent the average ± SD of 10 determinations. Excitation wavelength 488 nm. ^c Emission maximum of ligand bound to Aβ plaques (cores and coronas). ^d Calculated cLogP values using ChemDraw Ultra 12.0. ^e Measured for solute molecule in toluene.

Then, we measured the binding affinity of **4** to **7** towards Aβ1-42 fibrils and Aβ1-40 fibrils. As shown in Table 2 and Figure S5, the binding affinity of these probes, in conjuncture with **3c**, towards Aβ1-40 fibrils is weaker than towards Aβ1-42 fibrils, which is consistent with the low fluorescence intensity enhancement upon bound to Aβ1-40 fibrils. Therefore, we will focus on the binding affinity of these probes to Aβ1-42 fibrils. Compound **4** had the weakest binding affinity all the ligands, 26-fold weaker than that of **3c** and 3-fold less than that of DF-9. This could be attributed to the shorter distance between phenol functional groups, reducing the effectiveness of **4** to form strong H-bonds with the Aβ1-42 fibril binding pockets¹⁵. Compared to **3c**, the more rigid linear alkyne analogue **5** had a 2-fold lower Aβ1-42 fibril binding affinity, possibly due to an inability to attain a conformer orientation complementary to the binding pockets of the fibril but retained high

affinity (36 ± 3 nM). The order of the binding affinity of **3c**, **5**, **6** and **7** are consistent with the order of their emission maxima bound to A β 1-42 fibrils, demonstrating that the effective conjugation length will affect the binding affinity³⁰⁻³¹. However, compound **6** appear unsuitable for tissue staining (Figure S6). The same holds essentially true for compound **7**. While **7** can stain amyloid plaque in tissue (Figure S6) and has a >40 fold affinity for A β 1-42 over A β 1-40 fibrils, it has drawbacks. The intensity of compound **7** is rather weak. Its quantum yield is 0.29, it has merely 3.5 and 1.8-fold intensity difference bound to A β 1-42 and A β 1-40 fibrils compared to unbound probe, and small intensity differences over background for amyloid plaque. This property is likely related to its low affinity towards A β 1-40 fibrils, as was the case for **6** (Table 2).

BTDLigand staining and spectra implicates sensitivity towards A β amyloid polymorphism.

We next went back to tissue sections and assessed the binding specificity of the probes. Brain sections of an APP23 transgenic mouse (aged 19.5 months) was used for this purpose.³² Most importantly, APP23 mice at this age show a pronounced intrinsic amyloid plaque structural polymorphism³²⁻³⁴. We therefore selected this mouse model to assess the possibility of probing amyloid structural polymorphism by the ligands as implicated in the X-34, DF-9 and BTDSB co-staining experiments (Figure 1). By measuring the fluorescent intensities of A β plaques (specific signal) and background regions (noise, Figure 4 and S6) using the same fluorescence image, we first calculated a signal/noise (S/N) ratio, a measure of A β binding specificity.¹⁴⁻¹⁵ The notion that amyloid plaques are structurally polymorphic as one goes outward from the center has been reported previously for plaques formed in humans³⁵ and transgenic mice.³⁶ The binding specificity data were summarized in Tables 1-2. From the chemical perspective regarding to different spacers, **4**, **3c** and **7** could apparently stain A β plaque cores over A β plaque coronas. This is opposite for DF-9, which when used alone, preferentially stain A β plaque coronas rather than A β plaque cores

(Table 1, Figure S6). Surprisingly, **6** showed merely trace fluorescence signals from all A β plaque. Furthermore, on modifications on the outer phenyl rings using hydroxy and carboxyl motifs: i) **3c**, **3d**, **3f**, **3g**, **3i** and **3j** stain preferably A β plaque cores. ii) **3a**, **3b**, **3h** and BTDSB rather preferentially stain plaque coronas, iii) **3e** stain both plaque cores and plaque coronas. Interestingly, compared to the emission spectra of ligands bound to plaque coronas, the emission spectra of **5**, **3a**, **3c**, **3d** and **3e** bound to plaque cores were clearly blue-shifted (25, 16, 26, 19 and 21 nm, respectively). This indicates that the mature A β plaque cores have different binding sites or different binding site structures compared to coronal fibrils. The emission spectra of **4**, **7**, **3b**, **3f**, **3g**, **3h** and BTDSB merely slightly or did not show a blue-shift of the core compared to the corona. The comparison was especially striking for the symmetric **3c** versus **3h** versus **3j** which implicates a structure activity relationship (SAR)

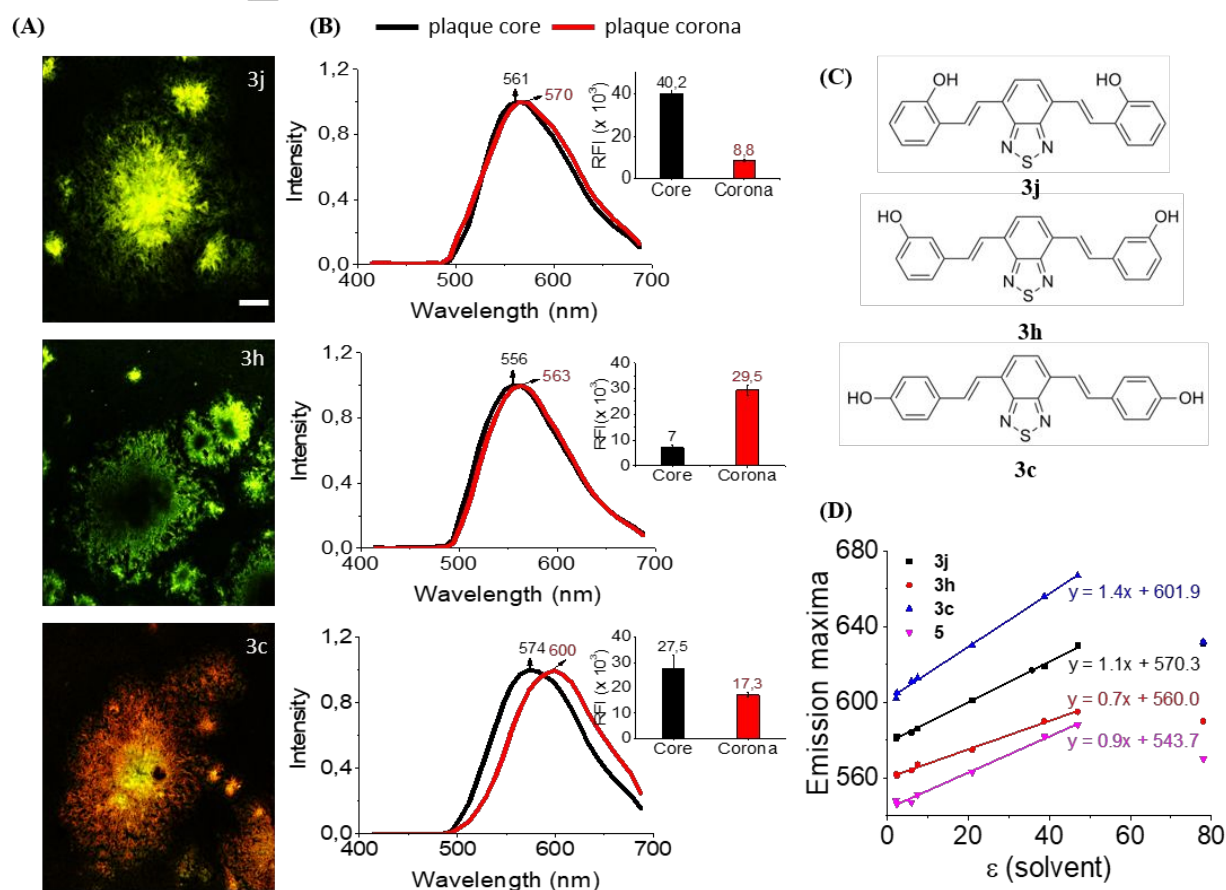


Figure 4. (A) Confocal images of mouse brain sections with accompanying normalized emission spectra (B) and the fluorescence intensity (inset) of **3j** and **3h** as well as **3c** bound to A β plaque core and plaque corona. 500 nM was used for all ligands, excitation 488 nm. Mouse brain sections are from an APP23 mouse (female, 19.5 months). Scale bars = 50 μ m. (C) Chemical structures of **3j**, **3h** and **3c**. (D) Emission maxima dependent on polarity of **3j**, **3h** and **3c** as well as **5** in different organic solvents (dioxane, toluene, EA, THF, acetone, DMF and DMSO) as well as in water. The apparent blue shift in water likely stems from limited solubility of the compounds in water.

conclusion: the *para*- and *ortho*-OH on the outer phenyl rings are sensitive to stain plaque cores while the *meta*-OH is to stain intensely plaque coronas (Figure 4A, 4B and 4C) Interestingly, fluorescence from **3c** bound to plaque core and corona could be easily discriminated by virtue of their spectra (Figure 4B)³⁶ This property was less pronounced for **3h** and **3j**. What is the basis for this variation? Testing **3c**, **3h** and **3j** in various solvents with decreasing dielectric constants reveals a linear dependence on the emission peak for all probes. The slope of emission peak versus dielectric constant was most pronounced for **3c** showing that variations in hydrophobicity is best sensed by **3c**. We therefore conclude that at least in part the observed amyloid plaque staining heterogeneity is explained by amyloid fibril binding site hydrophobicity, sensed most efficiently by **3c** (Figure 4D).

Given that *trans*-stilbenes are sensitive to cis-trans isomerization we noted that the alkyne analogue to **3c**, compound **5**, also showed this variation in spectra comparing the core with the corona of plaque (Table 2). As expected **5** showed a more pronounced slope of emission peak versus dielectric constant compared to **3h** (Figure 4D), analogous to **3c**.

CONCLUSIONS

Targeting amyloid by small molecule dyes for diagnostics and research is an intense research area moving towards new scaffolds to complement or replace Congo red and ThT.^{22,36-38} Recently the notion of amyloid targeting has focused on the realization that amyloid fibrils are polymorphic and behaves in a strain like manner which affect pathology and certainly should have bearing on amyloid fibril targeting.³⁹ Several studies have reported that combinations of multiple dyes can reveal A β amyloid plaque polymorphic heterogeneity in human AD.⁴⁰⁻⁴¹ Previous studies have reported Nile red,⁴² oligothiophenes,⁴³ ANCA⁴⁴ as single dyes with striking solvatochromic effects useful for amyloid fibril discrimination.

The structural basis for A β amyloid polymorphism has strong support by several structural models of both A β 1-40 and 1-42. This shows that A β amyloid fibrils generated under *in vitro* conditions are polymorphic⁴⁵ and can populate a variety of structures. These different folds and their respective assembly forms will generate different binding pockets for amyloid ligands.³⁹ It has been demonstrated that the bis-azo dye Congo red and anionic oligothiophenes binds in pockets outlined by lysine side chains.^{11, 46} We chose here-in to study a derivative inspired by the Congo red analogue X-34 because bis-styryl-benzene based Florbetaben and Florbetapir are currently approved for clinical diagnostics. In our study the BTDC center motif generates desirable red-shifted fluorescence properties important for broadening the research tool box. Importantly carboxylic acid functional groups (X-34 and BTDCSB) lower the binding affinity suggesting a diversion towards an alternative binding site compared to the Congo red type.⁴⁷ It is difficult to extrapolate *in vitro* polymorphic A β fibril structures towards *in vivo* A β amyloid plaque. Most ligands of our study preferred binding to A β 1-42 over A β 1-40 fibrils *in vitro*. The preferred binding site can therefore be assumed to be present in A β 1-42 fibrils. Recent model structures of A β 1-42 fibrils made under

similar conditions as used here display protomer folds resulting in a surface located C-terminal hydrophobic patch⁴⁵. It is tempting to speculate that this is the high affinity binding site for the neutral ligands of our study to *in vitro* fibrils. Amyloid deposits in APP23 mice are however dominated by A β 1-40. We have recently shown that in mature APP^{Swe} mice at 18 months (similar to APP23 mice used here) the diffuse amyloid plaque contains less A β 1-40 (10:1) compared to cored plaque (30:1).⁴⁸ However, most importantly, the core is highly packed. By extrapolation from DF-9 (neutral) binding in comparison to BTDSB (negatively charged) it appears that the core binding site is more hydrophobic and the periphery more charged of Congo red type. It has previously been shown in model fibril structures that the Congo red binding site is defined by a rack of positively charged lysines¹¹. We therefore speculate that the binding sites for core amyloid probes **3c** and **5** with para-OH on the phenyl rings is beneficial for binding affinity to tightly packed A β fibril polymorphs with buried Lys 16 and 28 and with accessible C-terminal hydrophobic binding sites. The peripheral plaque binding sites of the corona are in comparison dominated by polymorphs containing Congo red type binding sites. Variations in packing, called assembly polymorphism, and complexes with lipids may further contribute to the polarity variations observed within the core as sensitized by the **3c** type of probes reported here. It is noteworthy that the emission spectra obtained from the amyloid plaque appear exceptionally hydrophobic as derived from the solvent studies. Our ligands were designed with the aim to obtain planar neutral red shifted amyloid probe analogues. What we trade-off from the charged ligand is water solubility. While water solubility is often desirable for research purposes, presumably the neutral molecules would increase blood brain barrier penetration. For CNS penetrant molecules compared to other drugs an increased cLogP, less rotatable bonds, and fewer H-bonding partners are desirable⁴⁹. Such experiments are planned in future work. These data extend the SAR of BTD-based A β fibril targeting ligands and provide further direction for the development of A β fibril ligands for early

detection of AD. A new prototype based on 4,4'-((1E,1'E)-benzo[c][1,2,5]thiadiazole-4,7-diylbis(ethene-2,1-diyl))diphenol (**3c**) or 4,4'-(benzo[c][1,2,5]thiadiazole-4,7-diylbis(ethyne-2,1-diyl))diphenol (**5**) could serve coming designs and discoveries of new early diagnosis tools for AD and potentially for AD therapeutics.

EXPERIMENTAL SECTION

General information. All chemicals and solvents were obtained as reagent grade from conventional commercial sources and used without further purification unless otherwise noted. Thin-layer chromatography (TLC) was performed on Merck silica gel 60 F 254 (0.2 mm) on aluminum sheets using UV-light ($\lambda = 254$ nm and 366 nm). Nuclear magnetic resonance (NMR) spectra were recorded on a Varian Avance 300 MHz with solvent indicated. The ^1H NMR and ^{13}C NMR chemical shifts are reported in parts per million (ppm) relative to tetramethylsilane (TMS) or the residual solvent protons, ^1H NMR abbreviations for NMR data: s = singlet; d = doublet; t = triplet; dd = doublet of doublets; dt = doublet of triplets; m = multiplet. Coupling constants (J values) are given in hertz (Hz). Column chromatographic purification was carried out using silica gel 60 (particles size 0.040-0.063 mm). Compound purity is determined by high performance liquid chromatography (HPLC), and all final test compounds display purity higher than 95%. Analytical liquid chromatography was run on a Waters system equipped with a Waters 1525 gradient pump, 2998 Photodiode Array Detector, 2424 Evaporative Light Scattering Detector, SQD 2 Mass Detector and an Xbridge® C18 column (4.6×50 mm, 3.5 μm). A binary linear gradient of A/B 100:0 \rightarrow 0:100 over 4 min followed by an additional 2 min at 0:100 was used. Flow rate 1.5 mL/min. (A): 95:5 water:acetonitrile, 10 mM NH_4OAc pH 5.0; (B) 90:10 acetonitrile:water, 10 mM NH_4OAc pH 5.0. Preparative liquid chromatography was run on a Waters system equipped with a 2535 quaternary gradient pump, 2998 Photodiode Array Detector, 2424 Evaporative Light

Scattering Detector, SQD 2 Mass Detector and an xselect® phenyl-hexyl column (19 × 250 mm, 5.0 μm). Flow rate 25 mL/min. A binary linear gradient of A (95:5 water:acetonitrile, 10 mM NH₄OAc pH 5.0) and B (90:10 acetonitrile:water, 10 mM NH₄OAc pH 5.0) was used.

Synthesis of Phenolic bis-styrylbenzo[c]-1,2,5-thiadiazoles. A mixture of **1** (100 mg, 0.34 mmol), the corresponding (hydroxy)styrene component one (0.41 mmol), hydroxy-styrene component two (0.41 mmol), triethanolamine (203 mg, 1.36 mmol) and Pd(II)acetate (5.4 mg, 10%) in dry DMF (10 mL) was stirred under N₂ at 110 °C for 24 h. Then the mixture was cooled to room temperature, quenched by the addition of dil. aq. hydrochloride acid (0.5 N, 10 mL), and extracted with ethyl acetate (3 x 20 mL). The combined organic layers were concentrated in vacuo, and the crude product was purified by HPLC to give the target compounds.

4,7-di((E)-styryl)benzo[c][1,2,5]thiadiazole (3a)⁵⁰: 18% yield as red solid. ¹H NMR (300 MHz, Acetone-*d*₆) δ 7.31 – 7.36 (m, 2H), 7.42 – 7.47 (m, 4H), 7.71 – 7.80 (m, 6H), 7.92 (s, 2H), 8.16 (d, *J* = 16.5 Hz, 2H). ¹³C NMR (75 MHz, Acetone-*d*₆) δ 124.4, 126.8, 127.6, 128.1, 129.3, 133.3, 137.7, 153.8.

4-((E)-2-(7-((E)-styryl)benzo[c][1,2,5]thiadiazol-4-yl)vinyl) phenol (3b): 26% yield as red solid. ¹H NMR (300 MHz, Acetone-*d*₆) δ 6.92 (d, *J* = 8.7 Hz, 2H), 7.30 – 7.37 (m, 1H), 7.41 – 7.46 (m, 2H), 7.57 – 7.62 (m, 3H), 7.71 – 7.78 (m, 3H), 7.83 – 7.90 (m, 2H), 8.07 (d, *J* = 16.2 Hz, 1H), 8.14 (d, *J* = 16.2 Hz, 1H), 8.61 (s, OH) ¹³C NMR (75 MHz, Acetone-*d*₆) δ 115.7, 115.8, 121.4, 123.7, 124.6, 126.5, 126.7, 126.9, 127.6, 127.8, 128.0, 128.3, 128.5, 128.7, 128.8, 129.2, 129.9, 132.8, 133.3, 134.2, 137.7, 153.8, 158.0. HRMS (ESI, *m/z*): calcd for [M-H]⁻, 355.0905, found 355.0932.

4,4'-((1E,1'E)-benzo[c][1,2,5]thiadiazole-4,7-diylbis(ethene-2,1-diyl))diphenol (3c): 41% yield as red solid. ¹H NMR (300 MHz, Acetone-*d*₆) δ 6.92 (d, *J* = 8.4 Hz, 4H), 7.55 - 7.61 (m, 6H), 7.82 (d, *J* = 16.2 Hz, 4H), 8.59 (s, OH). ¹³C NMR (75 MHz, Acetone-*d*₆) δ 115.7, 121.6, 126.7, 128.2, 129.2, 129.3, 132.8, 153.8. HRMS (ESI, *m/z*): calcd for [M-H]⁻, 371.0854, found 371.0815.

4,4'-((1E,1'E)-benzo[c][1,2,5]thiadiazole-4,7-diylbis(ethene-2,1-diyl))bis(benzene-1,2-diol) (3d): 15% yield as red solid. ¹H NMR (300 MHz, Acetone-*d*₆) δ 6.88 (d, *J* = 8.1 Hz, 2H), 7.07 (dd, *J* = 8.1, 1.8 Hz, 2H), 7.24 (d, *J* = 1.8 Hz, 2H), 7.53 (d, *J* = 16.2 Hz, 2H), 7.81 (s, 2H), 7.97 (d, *J* = 16.2 Hz, 2H). ¹³C NMR (75 MHz, Acetone-*d*₆) δ 113.0, 115.5, 119.7, 121.6, 126.6, 129.1, 130.0, 133.0, 145.4, 145.9, 153.8. HRMS (ESI, *m/z*): calcd for [M-H]⁻, 403.0753, found 403.0730.

4-((E)-2-(7-((E)-4-hydroxystyryl)benzo[c][1,2,5]thiadiazol-4-yl)vinyl)benzene-1,2-diol (3e): 29% yield as red solid. ¹H NMR (300 MHz, Acetone-*d*₆) δ 6.87 – 6.93 (m, 3H), 7.06 (dd, *J* = 8.4, 1.8 Hz, 1H), 7.24 (d, *J* = 1.8 Hz, 1H), 7.50 – 7.60 (m, 4H), 7.81 (s, 2H), 7.96 (d, *J* = 16.2 Hz, 1H), 8.03 (d, *J* = 16.2 Hz, 1H). ¹³C NMR (75 MHz, Acetone-*d*₆) δ 115.5, 115.6, 115.7, 119.3, 119.7, 121.4, 121.6, 126.1, 126.6, 126.7, 128.2, 128.3, 129.1, 129.9, 130.0, 132.8, 133.1, 133.7, 153.8, 157.7. HRMS (ESI, *m/z*): calcd for [M-H]⁻, 387.0803, found 387.0814.

5,5'-((1E,1'E)-benzo[c][1,2,5]thiadiazole-4,7-diylbis(ethene-2,1-diyl))bis(benzene-1,3-diol) (3f): 12% yield as red solid. ¹H NMR (300 MHz, Acetone-*d*₆) δ 6.37 (s, 2H), 6.71 (d, *J* = 2.1 Hz, 4H), 7.64 (d, *J* = 16.5 Hz, 2H), 7.88 (s, 2H), 7.97 (d, *J* = 16.5 Hz, 2H), 8.30 (s, OH). ¹³C NMR (75 MHz, Acetone-*d*₆) δ 102.9, 105.3, 124.1, 127.3, 129.3, 133.4, 139.6, 153.8, 158.9. HRMS (ESI, *m/z*): calcd for [M-H]⁻, 403.0753, found 403.0798.

5-((E)-2-(7-((E)-4-hydroxystyryl)benzo[c][1,2,5]thiadiazol-4-yl)vinyl)benzene-1,3-diol (3g): 26% yield as red solid. ¹H NMR (300 MHz, Acetone-*d*₆) δ 6.37 (t, *J* = 2.1 Hz, 1H), 6.71 (d,

$J = 2.1$ Hz, 2H), 6.92 (d, $J = 8.4$ Hz, 2H), 7.54 – 7.65 (m, 4H), 7.79 – 7.86 (m, 2H), 7.93 (d, $J = 16.5$ Hz, 1H), 8.04 (d, $J = 16.5$ Hz, 1H). ^{13}C NMR (75 MHz, Acetone- d_6) δ 115.5, 115.6, 115.7, 119.3, 119.7, 121.4, 121.6, 126.1, 126.6, 126.7, 128.2, 128.3, 129.1, 129.9, 130.0, 132.8, 133.1, 133.7, 153.8, 157.7. HRMS (ESI, m/z): calcd for $[\text{M-H}]^-$, 387.0803, found 387.0770.

3,3'-((1E,1'E)-benzo[c][1,2,5]thiadiazole-4,7-diylbis(ethene-2,1-diyl))diphenol (3h): 9% yield as red solid. ^1H NMR (300 MHz, Acetone- d_6) δ 6.82 (dd, $J = 2.4, 1.2$, 1H), 6.84 (t, $J = 1.8$ Hz, 1H), 7.17 – 7.29 (m, 6H), 7.71 (d, $J = 16.2$ Hz, 2H), 7.89 (8s, 2H), 8.07 (d, $J = 16.2$ Hz, 2H), 8.40 (s, OH). ^{13}C NMR (75 MHz, Acetone- d_6) δ 113.2, 115.4, 118.5, 124.4, 127.3, 129.2, 129.8, 133.3, 139.0, 153.8, 157.8. HRMS (ESI, m/z): calcd for $[\text{M-H}]^-$, 371.0854, found 371.0829.

4-((E)-2-(7-((E)-3-hydroxystyryl)benzo[c][1,2,5]thiadiazol-4-yl)vinyl)benzene-1,2-diol (3i): 37% yield as red solid. ^1H NMR (300 MHz, Acetone- d_6) δ 6.82 (dt, $J = 7.8, 1.2$ Hz, 1H), 6.89 (d, $J = 8.1$ Hz, 1H), 7.07 (dd, $J = 8.1, 1.8$ Hz, 1H), 7.17 – 7.28 (m, 4H), 7.55 (d, $J = 16.5$ Hz, 1H), 7.69 (d, $J = 16.5$ Hz, 1H), 7.82 – 7.89 (m, 2H), 7.99 (d, $J = 16.5$ Hz, 1H), 8.05 (d, $J = 16.5$ Hz, 1H). ^{13}C NMR (75 MHz, Acetone- d_6) δ 113.0, 113.1, 115.2, 115.3, 115.6, 118.4, 119.8, 121.5, 124.4, 126.4, 127.6, 128.5, 129.7, 129.8, 130.0, 132.8, 133.5, 139.1, 145.4, 146.0, 153.8, 157.8. HRMS (ESI, m/z): calcd for $[\text{M-H}]^-$, 387.0853, found 387.0872.

2,2'-((1E,1'E)-benzo[c][1,2,5]thiadiazole-4,7-diylbis(ethene-2,1-diyl))diphenol (3j): 38% yield as red solid. ^1H NMR (300 MHz, Acetone- d_6) δ 6.93 – 6.99 (m, 4H), 7.14 – 7.19 (m, 2H), 7.73 (d, $J = 8.1$ Hz, 2H), 7.83 (d, $J = 16.5$ Hz, 2H), 7.89 (s, 2H), 8.41 (d, $J = 16.5$ Hz, 2H), 8.79 (s, OH). ^{13}C NMR (75 MHz, Acetone- d_6) δ 115.9, 119.9, 124.1, 124.7, 126.8, 126.9, 128.3, 129.1, 129.7, 153.9, 155.4. HRMS (ESI, m/z): calcd for $[\text{M-H}]^-$, 371.0854, found 371.0842.

Synthesis of 4,4'-(beno[c][1,2,5]thiadiazole-4,7-diyl)diphenol (4)⁵¹. To a mixture of **1** (100 mg, 0.34 mmol) and tetrakis(triphenylphosphine)palladium (11.8 mg, 3%) in toluene (10 mL) was added ethanol (5 mL) solution of **9** (94 mg, 0.68 mmol) and 2 M sodium carbonate solution (5 mL) at 60 °C under N₂ atmosphere. After the reaction mixture was heated at 90 °C for 12 h, it was poured into water (20 mL) and extracted with ethyl acetate (EA) (30 mL x 3). The combined organic layers were evaporated in vacuo to dryness. The residue was purified by silica gel column chromatography eluting with EA /*n*-hexane (1:3, v/v) to give **10** in 89% yield (92 mg, 0.30 mmol) as yellow solid.

To a mixture of **10** (40 mg, 0.13 mmol) and tetrakis(triphenylphosphine)palladium (4.4 mg, 3%) in toluene (10 mL) was added ethanol (5 mL) solution of **9** (36 mg, 0.26 mmol) and 2 M sodium carbonate solution (5 mL) at 60 °C under N₂ atmosphere. After the mixture was heated at 90 °C overnight, the reaction mixture was poured into water (10 mL) and extracted with EA (20 mL x 3). The combined organic layers were evaporated in vacuo to dryness. The residue was purified by silica gel column chromatography eluting with EA /*n*-hexane (1:2 to 1:1, v/v) to give **4** in 92% yield (37 mg, 0.12 mmol) as yellow solid. ¹H NMR (300 MHz, Acetone-*d*₆) δ 7.02 (d, *J* = 8.7 Hz, 4H), 7.84 (s, 2H), 7.95 (d, *J* = 8.7 Hz, 4H), 8.59 (s, OH). ¹³C NMR (75 MHz, Acetone-*d*₆) δ 115.3, 127.2, 128.8, 130.5, 132.1, 154.1, 157.7.

Synthesis of 4,4'-(benzo[c][1,2,5]thiadiazole-4,7 diylbis(ethyne-2,1 diyl))diphenol (5)⁵². A mixture of **12** (60 mg, 0.30 mmol) in 1 N potassium hydroxide methanol solution (10 mL) was stirred at room temperature for 1 h. The reaction mixture was poured into water (10 mL) and extracted with chloroform (15 mL x 3). The combined organic layers were evaporated in vacuo to dryness to give 4,7-diethynyl-2,1,3-benzothiadiazole (30 mg, 0.16 mmol) as brown powder. To a solution of this brown powder, 4-iodophenol (79 mg, 0.36 mmol), and triethylamine (113 μL) in

THF (10 mL) was added Pd(OAc)₂ (2.0 mg, 5%), PPh₃ (9.0 mg, 20%) and copper iodide (1.6 mg, 5%) under N₂ atmosphere. After the mixture was stirred at room temperature for 12 h, the reaction was poured into 1 N hydrochloric acid (10 mL) and extracted with dichloromethane (20 mL x 3). The combined organic layers were evaporated in vacuo to dryness. The residue was purified by silica gel column chromatography eluting with EA/*n*-hexane (1:2, v/v) to give **5** in 32% yield (19 mg, 0.051 mmol) as red solid. ¹H NMR (300 MHz, Acetone-*d*₆) δ 6.95 (d, *J* = 8.7 Hz, 4H), 7.54 (d, *J* = 8.7 Hz, 4H), 7.85 (s, 2H), 8.93 (s, OH). ¹³C NMR (75 MHz, Acetone-*d*₆) δ 83.9, 97.5, 113.4, 115.8, 117.0, 132.0, 133.4.

Synthesis of 4',4'''-(benzo[*c*][1,2,5]thiadiazole-4,7-diyl)bis([1'',1'''-biphenyl]-4-ol) (6**).** To a mixture of **1** (100 mg, 0.34 mmol) and tetrakis(triphenylphosphine)palladium (20 mg, 5%) in toluene (20 mL) were added ethanol (5 mL) solution of **16** (252 mg, 0.85 mmol) and 2 M sodium carbonate solution (5 mL) at 60 °C under N₂ atmosphere. After the mixture was heated at 85 °C for overnight, the reaction mixture was poured into water (20 mL) and extracted with EA (30 mL x 3). The combined organic layers were evaporated in vacuo to dryness. The residue was separated by silica gel column chromatography eluting with dichloromethane/*n*-hexane (1:1, v/v) to give **6** in 21% (34 mg, 0.07 mmol) as orange solid. ¹H NMR (300 MHz, DMSO-*d*₆) δ 6.90 (d, *J* = 8.1 Hz, 4H), 7.61 (d, *J* = 8.1 Hz, 4H), 7.75 (d, *J* = 8.1 Hz, 4H), 7.96 (s, 2H), 8.06 (d, *J* = 8.1 Hz, 4H), 9.66 (s, OH). ¹³C NMR (75 MHz, DMSO-*d*₆) δ 116.3, 126.4, 128.3, 130.0, 130.7, 132.1, 135.2, 140.5, 153.9, 157.9. HRMS (ESI, *m/z*): calcd for [M-H]⁻, 471.1167, found 471.1113.

Synthesis of 4,4'-(5,5'-(benzo[*c*][1,2,5]thiadiazole-4,7-diyl)bis(thiophene -5,2-diyl))diphenol (7**).** As described above for **4**, **19** (100 mg, 0.22 mmol) and **9** (90 mg, 0.65 mmol) yielded **7** in 46% yield (49 mg, 0.10 mmol) as deep-red solid. ¹H NMR (300 MHz, DMSO-*d*₆) δ 6.85 (d, *J* = 8.7 Hz, 4H), 7.46 (d, *J* = 3.9 Hz, 2H), 7.59 (d, *J* = 8.7 Hz, 4H), 8.07 (s, 2H), 8.13 (d, *J*

= 3.9 Hz, 2H). ^{13}C NMR (75 MHz, $\text{DMSO}-d_6$) δ 116.4, 123.3, 125.0, 125.1, 125.6, 127.3, 129.1, 136.6, 146.1, 152.1 158.1. HRMS (ESI, m/z): calcd for $[\text{M}-\text{H}]^-$, 483.0296, found 483.0324.

Optical characterization of ligands in organic solvent and water. Absorption and emission spectra of ligands in different solvents were collected using a Cary win UV 100 spectrophotometer and a Tecan Infinity M1000 microplate reader (Tecan, Männedorf, Switzerland), respectively.

Quantum yield determination. The quantum yields of DF-9 and BTDSB and its derivatives were measured in toluene. Dilute solutions (10^{-6} M) were used to minimize reabsorption effects. Fluorescence measurement were made three times for each ligand and averaged. Quantum yield was determined using the following equation:

$$\Phi_{\text{sample}} = \Phi_{\text{stand}} (F_{\text{sample}}/F_{\text{stand}}) \times (A_{\text{stand}} / A_{\text{sample}}) \times (n_{\text{sample}}^2/n_{\text{stand}}^2)$$

Where Φ = Quantum yield, F = Area under fluorescence spectra, A = Absorption maxima, and n = Refractive index. the reference for ligand **4** and **6** as well as DF-9 was Coumarin 314 in ethanol (Φ = 0.68) and fluorescein in 0.1M NaOH (Φ = 0.95) was used for all other compounds.

Fluorescence lifetime measurements. Fluorescence decays were performed using an IBH time-correlated single photo counting (TCSPC) spectrometer. The solution of each compound in toluene was degassed. After the sample solution was excited at each excitation wavelength, the fluorescence decay at emission maxima for each probe in toluene was monitored at room temperature. The instrument response function was determined with a fibril solution. Decay was fitted with a sum of exponentials (eq. 1) and the quality of the fit was determined from the χ^2 parameter and the random distribution of the residuals and the autocorrelation of the residuals.

$$I(t) = \sum_i \alpha_i \exp(-t/\tau_i) \quad (1)$$

Where α_i are the preexponential factors associated with the decay time τ_i . The average lifetime of fluorescence decay was calculated according to the following equation:

$$\tau_{avg} = \frac{\sum \alpha_i \tau_i^2}{\sum \alpha_i \tau_i} \quad (2)$$

Characterization of ligands towards recombinant A β 1-42 peptide (monomers and fibrils) and A β 1-40 peptide (monomers and fibrils). Recombinant A β 1-42 and 1-40 was expressed and purified using the system described by Linse and coworkers containing an additional methionine in the N-terminus.⁵³ Before the final step the lyophilized A β sample was solubilized in 6 M GuHCl before gel filtration on a Superdex 75 10/300 column (GE-Healthcare) in PBS buffer. Freshly monomeric gel filtered A β 1-42 and 1-40 was used in all experiments. A β 1-42 protein concentration was calculated using $\epsilon = 1490 \text{ M}^{-1} \text{ cm}^{-1}$ at 277 nm. The A β 1-42 and 1-40 fibrils were generated through incubation of 10 μM A β 1-42 and 1-40 at 37 $^{\circ}\text{C}$ in PBS buffer (pH 7.4) for 48 h under quiescent conditions and confirmed by thioflavin-T (ThT) staining.

Stock solutions of each ligand were made in DMSO. 1 μM of the respective ligand was added to 5 μM A β 1-42 peptide (monomers and fibrils) and A β 1-40 peptide (monomers and fibrils) in PBS and the excitation and emission spectra for each ligand were collected using a Tecan Sapphire microplate reader (Tecan, Männedorf, Switzerland). Both excitation and emission slit widths were 5 nm unless noted otherwise. The fold increase of the fluorescence intensity after binding to A β monomers or fibrils was calculated by the following equation:

$$\text{Fold increase (FI)} = \text{FI}_{\text{test}} / (\text{FI}_{\text{probe}} - \text{FI}_{\text{PBS}})$$

Where, FI_{test} , FI_{probe} and FI_{PBS} represent the fluorescence intensities of the ligands upon binding to A β 1-42 or A β 1-40 fibrils, the ligands in PBS, and PBS alone, respectively.

***In vitro* binding affinity determination by fluorescence titration.** A β 1-42 or A β 1-40 binding affinities (K_d) for **3 (3a-3j)**, **4**, **5**, **6**, **7** and BTDSB as well as DF-9 and X-34 were determined by means of fluorescence titrations.^{14, 22} Increasing concentration of ligand (0-400 nM) was titrated against a fixed concentration of fibrils (1 μ M) and the corresponding fluorescence spectra were recorded until the fluorescence no longer increased (saturation) by the Infinity M1000 plate reader (Tecan, Männedorf, Switzerland) using excitation wavelength determined for each compound. The K_d binding curves were generated by GraphPad Prism 7.0 by using below equation,

$$Y = B_{\max} * X / (K_d + X)$$

where X is concentration of ligand and Y is change in fluorescence intensity. B_{\max} is the maximum specific binding having the same unit as Y.

***Ex vivo* plaque binding specificity using APP23 transgenic mouse brain sections.** Frozen brain sections (10 μ m) from APP23 mouse brain tissues from a 19.5 months old female⁵⁴ were fixed in 98% EtOH, rehydrated in 50% EtOH and dH₂O and then incubated in PBS for 10 min. Probes were diluted to 500 nM in PBS and added to the sections. After 1 h, the sections were washed with PBS and mounted with DaKo fluorescent mounting medium (DaKo Cytomation, Glostrup, Denmark). The mounting medium was allowed to solidify over night before collecting emission spectral images from cortical plaques using an inverted LSM 780 confocal microscope (Carl Zeiss, Oberkochen, Germany) with 405 nm (DF-9, X-34) or 488 nm (all other probes) as excitation wavelengths.

ASSOCIATED CONTENT

Supporting Information. The supporting information is available on the ACS Publications website at: XXX. SI items: Molecular Formula Strings, and Supporting Figures S1-S6, Supporting Tables S1-S3, and NMR spectra of all target molecules.

AUTHOR INFORMATION

Corresponding Author

Per Hammarström

Division of chemistry, Department of Physics, Chemistry and Biology

Linköping University, 581 83 Linköping, Sweden

E-mail: per.hammarstrom@liu.se

Author Contributions

The study was conceived by JZ, XW, PK and PH. JZ, AK, AS, XW, SN, PK, ML, PH performed research and analyzed data. UO and BWB provided samples. The manuscript draft was written by JZ and PH. All authors have given approval to the final version of the manuscript.

Funding Sources

Our work was funded by the China Scholarship Council, the Swedish Research Council (2015-04521), the Göran Gustafsson Foundation, the Swedish Alzheimer Foundation, the Swedish Brain foundation, and Linköping University (LiU-Neuro).

Notes

Any additional relevant notes should be placed here.

ACKNOWLEDGMENT

We acknowledge Peter Nilsson for discussions on fluorescence microscopy and Mathias Jucker for discussions and assistance with APP23 tissue handling.

ABBREVIATIONS

AD, Alzheimer's disease; TLC, thin layer chromatography.

REFERENCES

- (1) Goedert, M.; Spillantini, M. G. A century of Alzheimer's disease. *Science* **2006**, *314*, 777-781.
- (2) Prince, M.; Bryce, R.; Albanese, E.; Wimo, A.; Ribeiro, W.; Ferri, C. P. The global prevalence of dementia: a systematic review and metaanalysis. *Alzheimers Dement.* **2013**, *9*, 63-75.
- (3) Hamley, I. W. The amyloid beta peptide: a chemist's perspective. role in Alzheimer's and fibrillization. *Chem. Rev.* **2012**, *112*, 5147-5192.
- (4) Nisbet, R. M.; Polanco, J.-C.; Ittner, L. M.; Götz, J. Tau aggregation and its interplay with amyloid- β . *Acta Neuropathol.* **2015**, *129*, 207-220.
- (5) Iqbal, K.; Liu, F.; Gong, C. X. Alzheimer disease therapeutics: Focus on the disease and not just plaques and tangles. *Biochem. Pharmacol.* **2014**, *88*, 631-639.
- (6) Kung, H. F.; Lee, C. W.; Zhuang, Z. P.; Kung, M. P.; Hou, C.; Plössl, K. Novel stilbenes as probes for amyloid plaques. *J. Am. Chem. Soc.* **2001**, *123*, 12740-12741.
- (7) Nesterov, E. E.; Skoch, J.; Hyman, B. T.; Klunk, W. E.; Bacskai, B. J.; Swager, T. M. In vivo optical imaging of amyloid aggregates in brain: Design of fluorescent markers. *Angew. Chem. Int. Ed.* **2005**, *44*, 5452-5456.
- (8) Shozo, F.; Nobuyuki, O.; Ren, I.; Kazuhiko, Y.; Hiroyuki, A.; Yukitsuka, K. Recent advances in the development of amyloid imaging agents. *Curr. Top. Med. Chem.* **2007**, *7*, 1773-1789.
- (9) Nilsson, K. P. R. Small organic probes as amyloid specific ligands – past and recent molecular scaffolds. *FEBS Lett.* **2009**, *583*, 2593-2599.
- (10) Scot D. Styren; Hamilton, R. L.; Styren, G. C.; Klunk, W. E. X-34, a fluorescent derivative of Congo red: a novel histochemical stain for Alzheimer's disease. *J. Histochem. Cytochem.* **2000**, *48*, 1223-1232.

- (11) Schütz, A. K.; Soragni, A.; Hornemann, S.; Aguzzi, A.; Ernst, M.; Böckmann, A.; Meier, B. H. The amyloid–Congo red interface at atomic resolution. *Angew. Chem. Int. Ed.* **2011**, *50*, 5956-5960.
- (12) Crystal, A. S.; Giasson, B. I.; Crowe, A.; Kung, M. P.; Zhuang, Z. P.; Trojanowski, J. Q.; Lee, V. M. A comparison of amyloid fibrillogenesis using the novel fluorescent compound K114. *J. Neurochem.* **2003**, *86*, 1359-1368.
- (13) LeVine, H., 3rd. Mechanism of A β (1-40) fibril-induced fluorescence of (trans,trans)-1-bromo-2,5-bis(4-hydroxystyryl)benzene (K114). *Biochemistry* **2005**, *44*, 15937-15943.
- (14) Flaherty, D. P.; Walsh, S. M.; Kiyota, T.; Dong, Y.; Ikezu, T.; Vennerstrom, J. L. Polyfluorinated bis-styrylbenzene β -amyloid plaque binding ligands. *J. Med. Chem.* **2007**, *50*, 4986-4992.
- (15) Flaherty, D. P.; Kiyota, T.; Dong, Y.; Ikezu, T.; Vennerstrom, J. L. Phenolic bis-styrylbenzenes as β -amyloid binding ligands and free radical scavengers. *J. Med. Chem.* **2010**, *53*, 7992-7999.
- (16) Klunk, W. E.; Bacskai, B. J.; Mathis, C. A.; Kajdasz, S. T.; McLellan, M. E.; Frosch, M. P.; Debnath, M. L.; Holt, D. P.; Wang, Y.; Hyman, B. T. Imaging A β plaques in living transgenic mice with multiphoton microscopy and methoxy-X04, a systemically administered Congo red derivative. *J. Neuropathol. Exp. Neurol.* **2002**, *61*, 797-805.
- (17) Hefendehl, J. K.; Wegenast-Braun, B. M.; Liebig, C.; Eicke, D.; Milford, D.; Calhoun, M. E.; Kohsaka, S.; Eichner, M.; Jucker, M. Long-term in vivo imaging of β -amyloid plaque appearance and growth in a mouse model of cerebral β -amyloidosis. *J. Neurosci.* **2011**, *31*, 624-629.

- (18) Hefendehl, J. K.; Milford, D.; Eicke, D.; Wegenast-Braun, B. M.; Calhoun, M. E.; Grathwohl, S. A.; Jucker, M.; Liebig, C. Repeatable target localization for long-term in vivo imaging of mice with 2-photon microscopy. *J. Neurosci. Methods* **2012**, *205*, 357-363.
- (19) Neto, B. A. D.; Carvalho, P. H. P. R.; Correa, J. R. Benzothiadiazole derivatives as fluorescence imaging probes: beyond classical scaffolds. *Acc. Chem. Res.* **2015**, *48*, 1560-1569.
- (20) Dyrager, C.; Vieira, R. P.; Nystrom, S.; Nilsson, K. P. R.; Storr, T. Synthesis and evaluation of benzothiazole-triazole and benzothiadiazole-triazole scaffolds as potential molecular probes for amyloid- β aggregation. *New J. Chem.* **2017**, *41*, 1566-1573.
- (21) Shirani, H.; Linares, M.; Sigurdson, C. J.; Lindgren, M.; Norman, P.; Nilsson, K. P. A palette of fluorescent thiophene-based ligands for the identification of protein aggregates. *Chemistry* **2015**, *21*, 15133-15137.
- (22) Zhang, J.; Sandberg, A.; Konsmo, A.; Wu, X.; Nyström, S.; Nilsson, K. P. R.; Konradsson, P.; LeVine, H.; Lindgren, M.; Hammarström, P. Detection and imaging of A β 1-42 and Tau fibrils by redesigned fluorescent X-34 analogues. *Chem. Eur. J.* **2018**, *24*, 7210-7216.
- (23) Nyström, S.; Psonka-Antonczyk, K. M.; Ellingsen, P. G.; Johansson, L. B. G.; Reitan, N.; Handrick, S.; Prokop, S.; Heppner, F. L.; Wegenast-Braun, B. M.; Jucker, M.; Lindgren, M.; Stokke, B. T.; Hammarström, P.; Nilsson, K. P. R. Evidence for age-dependent in vivo conformational rearrangement within A β amyloid deposits. *ACS Chem. Biol.* **2013**, *8*, 1128-1133.
- (24) Psonka-Antonczyk, K. M.; Hammarstrom, P.; Johansson, L. B.; Lindgren, M.; Stokke, B. T.; Nilsson, K. P.; Nystrom, S. Nanoscale structure and spectroscopic probing of A β 1-40 fibril bundle formation. *Front Chem.* **2016**, *4*, 44.
- (25) Zhang, J.; Sandberg, A.; Wu, X. Y.; Nyström, S.; Lindgren, M.; Konradsson, P.; Hammarström, P. Trans-stilbenoids with extended fluorescence lifetimes for the characterization of amyloid fibrils. *ACS Omega* **2017**, *2*, 4693-4704.

(26) Kato, S. i.; Matsumoto, T.; Ishi-i, T.; Thiemann, T.; Shigeiwa, M.; Gorohmaru, H.; Maeda, S.; Yamashita, Y.; Ma-taka, S. Strongly red-fluorescent novel donor- π -bridge-acceptor- π -bridge-donor (D- π -A- π -D) type 2,1,3-benzothiadiazoles with enhanced two-photon absorption cross-sections. *Chem. Comm.* **2004**, 2342-2343.

(27) Zhang, X.; Yamaguchi, R.; Moriyama, K.; Kadowaki, M.; Kobayashi, T.; Ishi-i, T.; Thiemann, T.; Mataka, S. Highly dichroic benzo-2,1,3-thiadiazole dyes containing five linearly π -conjugated aromatic residues, with fluorescent emission ranging from green to red, in a liquid crystal guest-host system. *J Mater. Chem*, **2006**, 16, 736 – 740.

(28) Xue, S.; Liu, S.; He, F.; Yao, L.; Gu, C.; Xu, H.; Xie, Z.; Wu, H.; Ma, Y. Chemistry and materials based on 5,5[prime or minute]-bibenzo[c][1,2,5]thiadiazole. *Chem. Comm.* **2013**, 49, 5730-5732.

(29) Croce, A. C.; Bottirolì, G. Autofluorescence spectroscopy and imaging: a tool for biomedical research and diagnosis. *Eur. J. Histochem.* **2014**, 58, 2461.

(30) Cui, M.; Ono, M.; Watanabe, H.; Kimura, H.; Liu, B.; Saji, H. Smart near-infrared fluorescence probes with donor–acceptor structure for in vivo detection of β -amyloid deposits. *J. Am. Chem. Soc.* **2014**, 136, 3388-3394.

(31) Zhou, K.; Fu, H.; Feng, L.; Cui, M.; Dai, J.; Liu, B. The synthesis and evaluation of near-infrared probes with barbituric acid acceptors for in vivo detection of amyloid plaques. *Chem. Comm.* **2015**, 51, 11665-11668.

(32) Sturchler-Pierrat, C.; Abramowski, D.; Duke, M.; Wiederhold, K. H.; Mistl, C.; Rothacher, S.; Ledermann, B.; Bürki, K.; Frey, P.; Paganetti, P. A.; Waridel, C.; Calhoun, M. E.; Jucker, M.; Probst, A.; Staufenbiel, M.; Sommer, B. Two amyloid precursor protein transgenic mouse models with Alzheimer disease-like pathology. *Proc. Natl. Acad. Sci. U.S.A.* **1997**, 94, 13287-13292.

- (33) Radde, R.; Bolmont, T.; Kaeser, S. A.; Coomaraswamy, J.; Lindau, D.; Stoltze, L.; Calhoun, M. E.; Jaggi, F.; Wolburg, H.; Gengler, S.; Haass, C.; Ghetti, B.; Czech, C.; Holscher, C.; Mathews, P. M.; Jucker, M. Abeta42-driven cerebral amyloidosis in transgenic mice reveals early and robust pathology. *EMBO Rep.* **2006**, *7*, 940-946.
- (34) Lord, A.; Philipson, O.; Klingstedt, T.; Westermark, G.; Hammarstrom, P.; Nilsson, K. P.; Nilsson, L. N. Observations in APP bitransgenic mice suggest that diffuse and compact plaques form via independent processes in Alzheimer's disease. *Am. J. Pathol.* **2011**, *178*, 2286-2298.
- (35) Jin, L. W.; Claborn, K. A.; Kurimoto, M.; Geday, M. A.; Maezawa, I.; Sohraby, F.; Estrada, M.; Kaminsky, W.; Kahr, B. Imaging linear birefringence and dichroism in cerebral amyloid pathologies. *Proc. Natl. Acad. Sci. U.S.A.* **2003**, *100*, 15294-15298.
- (36) Nystrom, S.; Psonka-Antonczyk, K. M.; Ellingsen, P. G.; Johansson, L. B.; Reitan, N.; Handrick, S.; Prokop, S.; Heppner, F. L.; Wegenast-Braun, B. M.; Jucker, M.; Lindgren, M.; Stokke, B. T.; Hammarstrom, P.; Nilsson, K. P. Evidence for age-dependent in vivo conformational rearrangement within A β amyloid deposits. *ACS Chem. Biol.* **2013**, *8*, 1128-1133.
- (37) Aslund, A.; Sigurdson, C. J.; Klingstedt, T.; Grathwohl, S.; Bolmont, T.; Dickstein, D. L.; Glimsdal, E.; Prokop, S.; Lindgren, M.; Konradsson, P.; Holtzman, D. M.; Hof, P. R.; Heppner, F. L.; Gandy, S.; Jucker, M.; Aguzzi, A.; Hammarstrom, P.; Nilsson, K. P. Novel pentameric thiophene derivatives for in vitro and in vivo optical imaging of a plethora of protein aggregates in cerebral amyloidoses. *ACS Chem. Biol.* **2009**, *4*, 673-684.
- (38) Sjolander, D.; Bijzet, J.; Hazenberg, B. P.; Nilsson, K. P.; Hammarstrom, P. Sensitive and rapid assessment of amyloid by oligothiophene fluorescence in subcutaneous fat tissue. *Amyloid* **2015**, *22*, 19-25.

- (39) Fandrich, M.; Nystrom, S.; Nilsson, K. P. R.; Bockmann, A.; LeVine, H., 3rd; Hammarstrom, P. Amyloid fibril polymorphism: a challenge for molecular imaging and therapy. *J. Intern. Med.* **2018**, *283*, 218-237.
- (40) Rasmussen, J.; Mahler, J.; Beschorner, N.; Kaeser, S. A.; Hasler, L. M.; Baumann, F.; Nystrom, S.; Portelius, E.; Blennow, K.; Lashley, T.; Fox, N. C.; Sepulveda-Falla, D.; Glatzel, M.; Oblak, A. L.; Ghetti, B.; Nilsson, K. P. R.; Hammarstrom, P.; Staufenbiel, M.; Walker, L. C.; Jucker, M. Amyloid polymorphisms constitute distinct clouds of conformational variants in different etiological subtypes of Alzheimer's disease. *Proc. Natl. Acad. Sci. U. S. A.* **2017**, *114*, 13018-13023.
- (41) Condello, C.; Lemmin, T.; Stohr, J.; Nick, M.; Wu, Y.; Maxwell, A. M.; Watts, J. C.; Caro, C. D.; Oehler, A.; Keene, C. D.; Bird, T. D.; van Duinen, S. G.; Lannfelt, L.; Ingelsson, M.; Graff, C.; Giles, K.; DeGrado, W. F.; Prusiner, S. B. Structural heterogeneity and intersubject variability of A β in familial and sporadic Alzheimer's disease. *Proc. Natl. Acad. Sci. U. S. A.* **2018**, *115*, 782-791.
- (42) Mishra, R.; Sjolander, D.; Hammarstrom, P. Spectroscopic characterization of diverse amyloid fibrils in vitro by the fluorescent dye Nile red. *Mol. Biosyst.* **2011**, *7*, 1232-1240.
- (43) Klingstedt, T.; Shirani, H.; Aslund, K. O.; Cairns, N. J.; Sigurdson, C. J.; Goedert, M.; Nilsson, K. P. The structural basis for optimal performance of oligothiophene-based fluorescent amyloid ligands: conformational flexibility is essential for spectral assignment of a diversity of protein aggregates. *Chemistry* **2013**, *19*, 10179-10192.
- (44) Cao, K. J.; Elbel, K. M.; Cifelli, J. L.; Cirera, J.; Sigurdson, C. J.; Paesani, F.; Theodorakis, E. A.; Yang, J. Solvation-guided design of fluorescent probes for discrimination of amyloids. *Sci. Rep.* **2018**, *8*, 6950.

- (45) Walti, M. A.; Ravotti, F.; Arai, H.; Glabe, C. G.; Wall, J. S.; Bockmann, A.; Guntert, P.; Meier, B. H.; Riek, R. Atomic-resolution structure of a disease-relevant A β (1-42) amyloid fibril. *Proc. Natl. Acad. Sci. U. S. A.* **2016**, *113*, 4976-4984.
- (46) Schutz, A. K.; Hornemann, S.; Walti, M. A.; Greuter, L.; Tiberi, C.; Cadalbert, R.; Gantner, M.; Riek, R.; Hammarstrom, P.; Nilsson, K. P. R.; Bockmann, A.; Aguzzi, A.; Meier, B. H. Binding of polythiophenes to amyloids: structural mapping of the pharmacophore. *ACS Chem. Neurosci.* **2018**, *9*, 475-481.
- (47) LeVine, H., 3rd. Multiple ligand binding sites on A β (1-40) fibrils. *Amyloid* **2005**, *12*, 5-14.
- (48) Michno, W.; Kaya, I.; Nyström, S.; Guerard, L.; Nilsson, K. P. R.; Hammarström, P.; Blennow, K.; Zetterberg, H.; Hanrieder, J. Multimodal chemical imaging of amyloid plaque polymorphism reveals A β aggregation dependent anionic lipid accumulations and metabolism. *Anal. Chem.* **2018**, *90*, 8130-8138.
- (49) Pajouhesh H, Lenz GR. Medicinal chemical properties of successful central nervous system drugs. *NeuroRx*. **2005**, *4*, 541-553.
- (50) Tobin, J. M.; McCabe, T. J. D.; Prentice, A. W.; Holzer, S.; Lloyd, G. O.; Paterson, M. J.; Arrighi, V.; Cormack, P. A. G.; Vilela, F. Polymer-supported photosensitizers for oxidative organic transformations in flow and under visible light irradiation. *ACS Catal.* **2017**, *7*, 4602-4612.
- (51) Omer, K. M.; Ku, S. Y.; Wong, K. T.; Bard, A. J. Green electrogenerated chemiluminescence of highly fluorescent benzothiadiazole and fluorene derivatives. *J. Am. Chem. Soc.* **2009**, *131*, 10733-10741.
- (52) Dong, Y.; Koken, B.; Ma, X.; Wang, L.; Cheng, Y.; Zhu, C. Polymer-based fluorescent sensor incorporating 2,2-bipyridyl and benzo[2,1,3]thiadiazole moieties for Cu²⁺ detection. *Inorg. Chem. Commun.* **2011**, *14*, 1719-1722.

(53) Walsh, D. M.; Thulin, E.; Minogue, A. M.; Gustavsson, N.; Pang, E.; Teplow, D. B.; Linse, S. A facile method for expression and purification of the Alzheimer's disease-associated amyloid β -peptide. *FEBS J.* **2009**, *276*, 1266-1281.

(54) Sturchler-Pierrat, C.; Abramowski, D.; Duke, M.; Wiederhold, K. H.; Mistl, C.; Rothacher, S.; Ledermann, B.; Burki, K.; Frey, P.; Paganetti, P. A.; Waridel, C.; Calhoun, M. E.; Jucker, M.; Probst, A.; Staufenbiel, M.; Sommer, B. Two amyloid precursor protein transgenic mouse models with Alzheimer disease-like pathology. *Proc. Natl. Acad. Sci. U. S. A.* **1997**, *94*, 13287-13292.

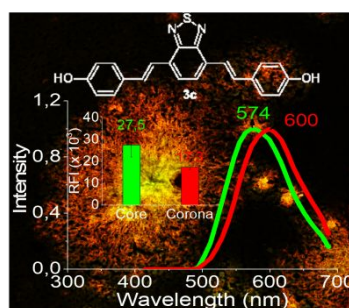


Table of Contents graphic

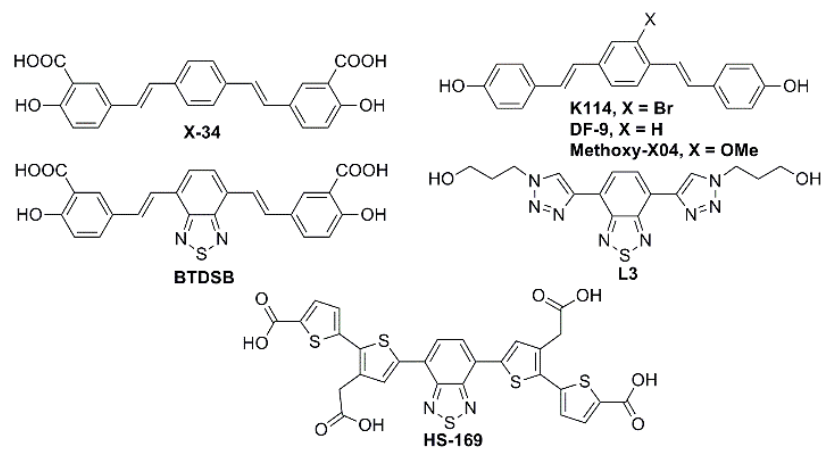


Chart 1. Chemical structures of amyloid ligands reported previously.

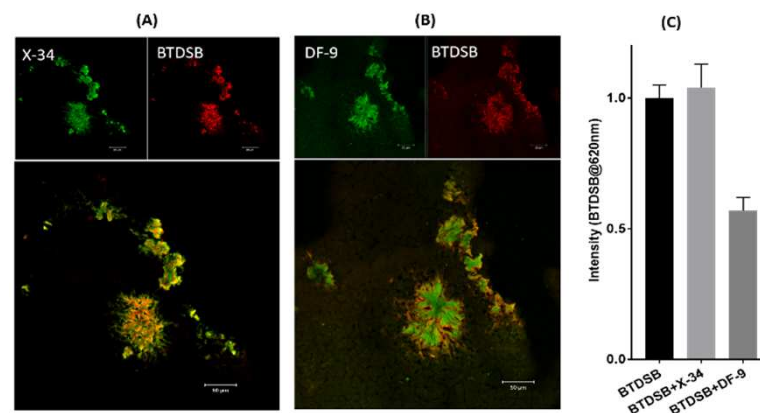
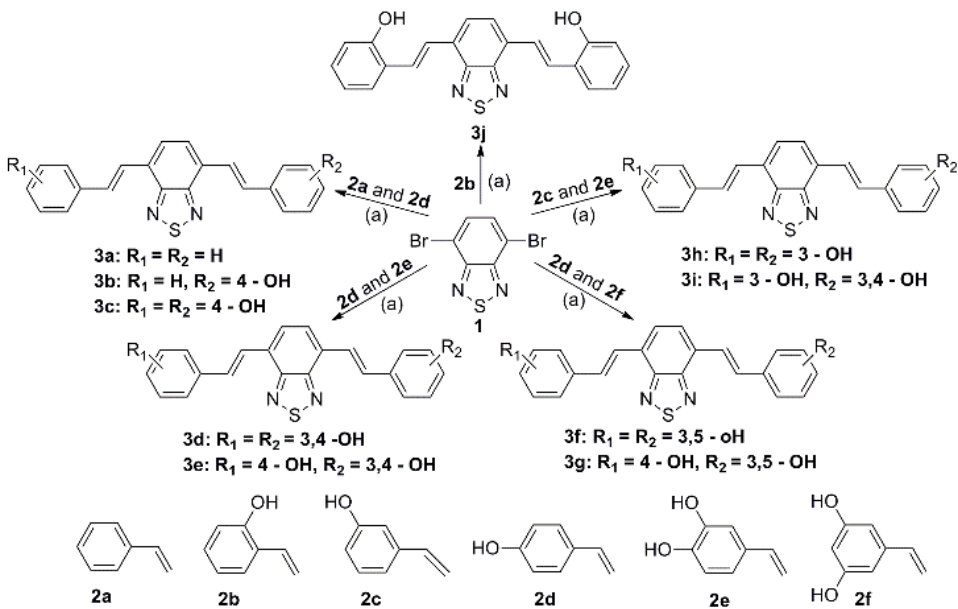


Figure 1. (A) Single plane confocal images of APP23 mouse brain sections (female, 19.5 months) after co-staining with X-34 and BTDSB (top) and the merged image of X-34 and BTDSB (down). (B) after co-staining with DF-9 and BTDSB (top) and the merged image of DF-9 and BTDSB (down). Z-depth was selected for the center of the largest plaque. (C) Competition assays using BTDSB (500 nM) to displace X-34 (or DF-9) in the presence of A β 1-40 fibrils (5 μ M) *in vitro* in PBS (pH 7.4).

Scheme 1. Synthesis of BTDSB derivatives



Conditions and reagents: (a) $Pd(OAc)_2$, triethanolamine, DMF.

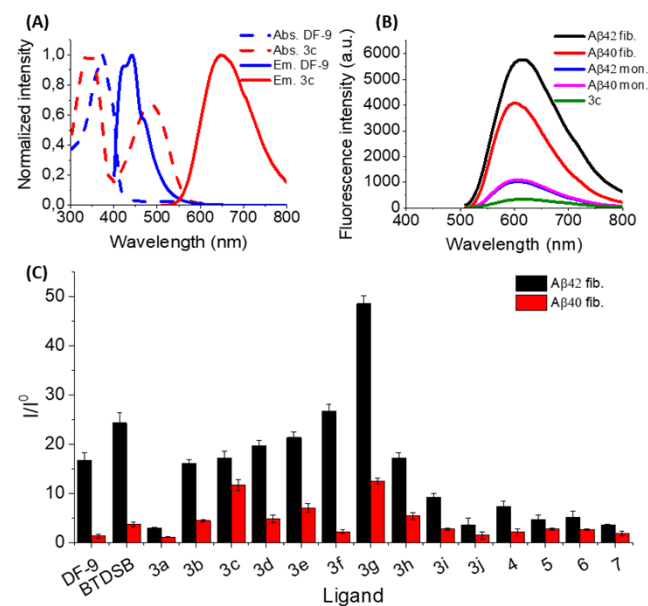
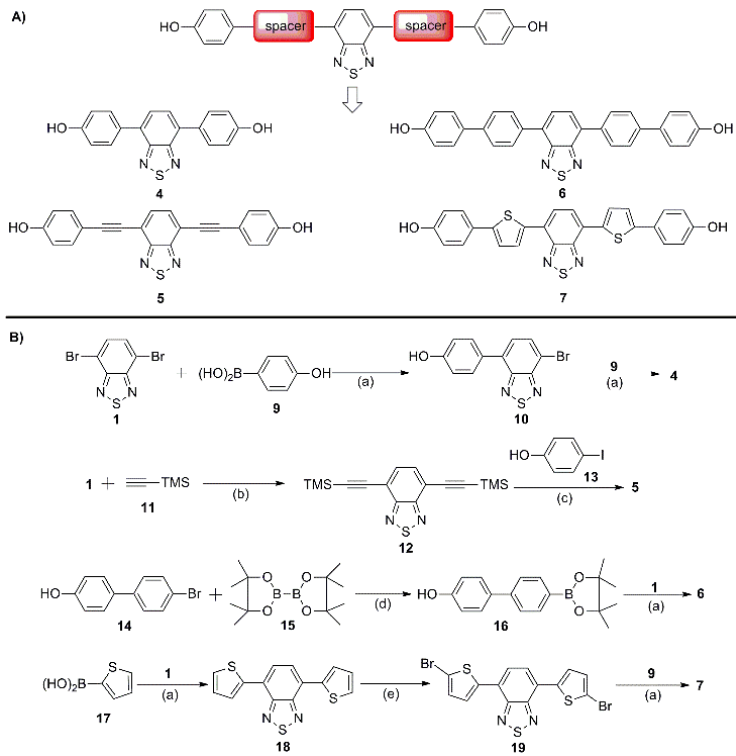


Figure 2. (A) Normalized absorption (dashed) and emission (solid) spectra of DF-9 (blue) and 3c (red) with 2 μ M in DMSO. (B) Emission spectra of 3c in the absence or presence of A β 1-42 and A β 1-40 peptides (monomers and fibrils) in PBS buffer. (C) Fluorescence intensity enhancements of 3a to 3j and BTDSB as well as DF-9 as control when bound to A β 1-42 or A β 1-40 fibrils compared to free in solution. Excitation wavelengths: 360 nm for DF-9, 430 nm for 4, 460 nm for 3a, 3h, 3f, 5, 6, and 490 nm for all other ligands.

Scheme 2. Synthesis of BTd derivatives with different conjugated spacers^a



^a Conditions and reagents: (a) Pd(PPh₃)₄, 2M Na₂CO₃, benzene-EtOH, 90 °C; (b) Pd(PPh₃)₄, CuI, triethylamine, 75 °C; (c) 1) KOH in MeOH, rt; 2) Pd(OAc)₂, PPh₃, CuI, triethylamine, THF, rt; (d) PdCl₂(dppf), dppf, KOAc, 1,4-dioxane, 90 °C; (e) NBS, CHCl₃, rt.

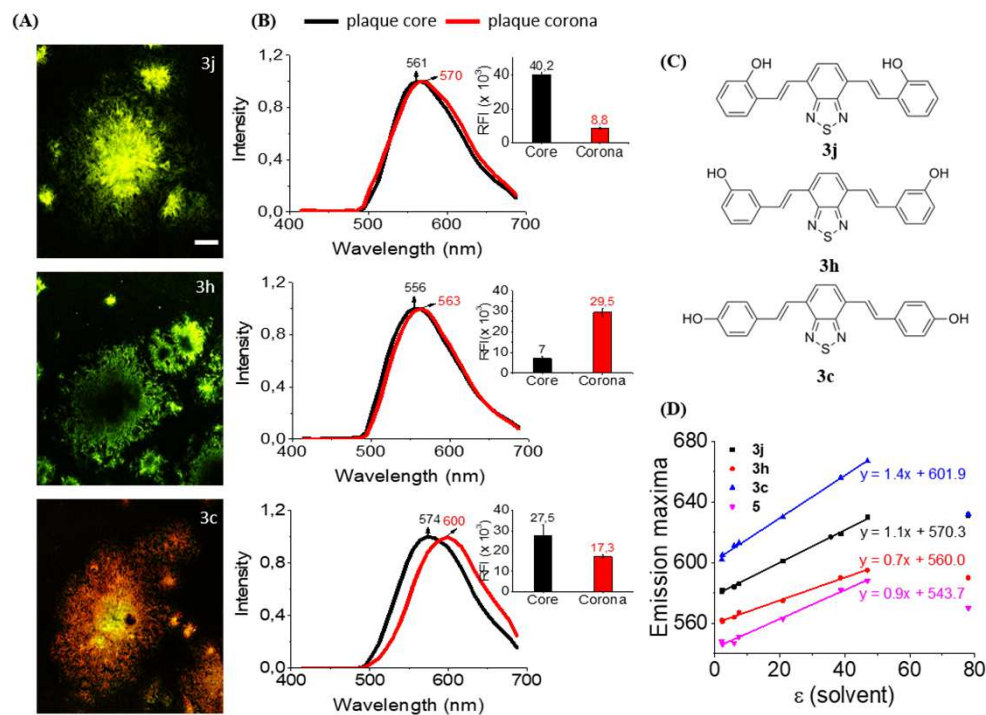
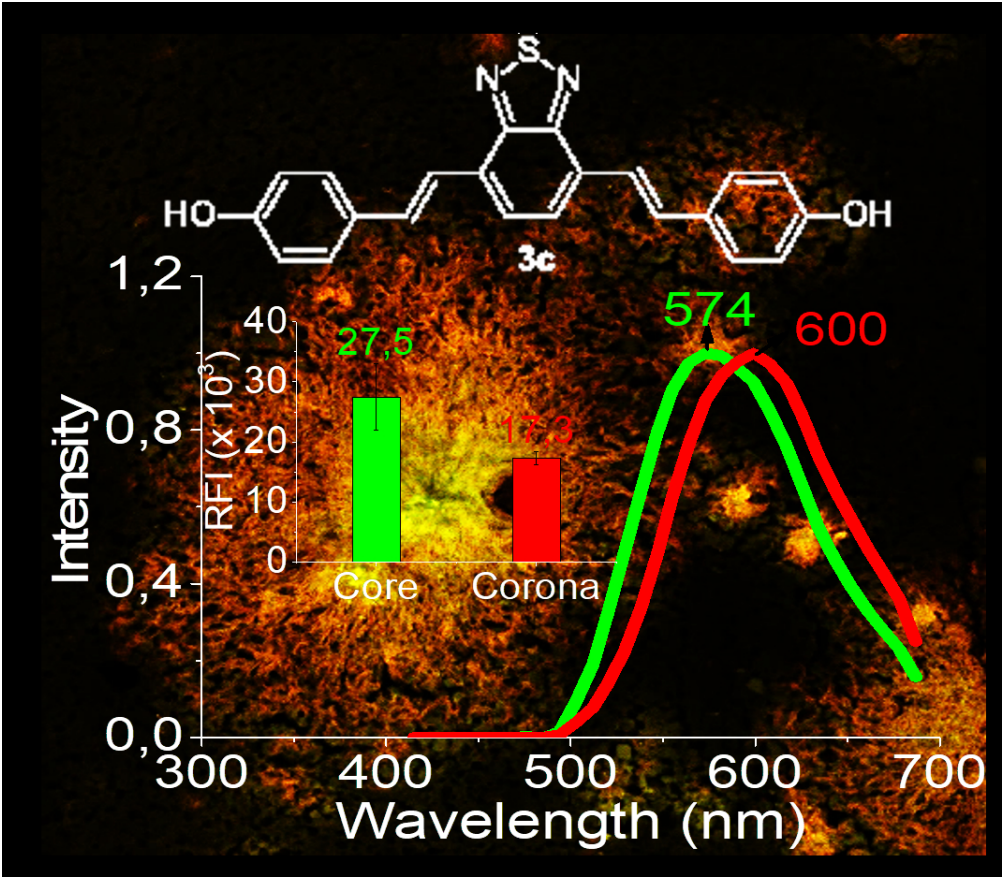


Figure 4. (A) Confocal images of mouse brain sections with accompanying normalized emission spectra (B) and the fluorescence intensity (inset) of **3j** and **3h** as well as **3c** bound to Aβ plaque core and plaque corona. 500 nm was used for all ligands. Mouse brain sections are from an APP23 mouse (female, 19.5 months). Scale bars = 50 μm. (C) Chemical structures of **3j**, **3h** and **3c**. (D) Emission maxima dependent on polarity of **3j**, **3h** and **3c** as well as **5** in different organic solvents (dioxane, toluene, EA, THF, acetone, DMF and DMSO) as well as in water. The apparent blue shift in water likely stems from limited solubility of the compounds in water.



180x158mm (150 x 150 DPI)